

Manufacturing of a fiber optic Young's double pinhole interferometer for use as a 3-D profilometer

Timothy L. Pennington, Anbo Wang, Hai Xiaio,
and Russell May

*Photonics Laboratory,
Bradley Department of Electrical and Computer Engineering,
Virginia Polytechnic Institute and State University,
Blacksburg, VA 24061*

*penningt@ee.vt.edu, awang@vt.edu
<http://www.ee.vt.edu/~photonics>*

Abstract: The method used to manufacture a Young's double pinhole interferometer is discussed. This interferometer is destined to be used in a surface profilometer using two wavelengths so that the zero order fringe can be determined. Hence stringent requirements are placed on the absolute length difference between the two output fibers of a single mode coupler. These requirements are discussed along with the manufacturing process. The interferometer is shown along with measurements showing a length difference on the order of $6\mu\text{m}$.

© 2000 Optical Society of America

OCIS codes: (060.1810) Fiber Optic Couplers; (120.6650) Surface Measurements; (150.6910) Three-dimensional sensing

References and links

1. G. Indebetouw, "Profile measurement using projection of running fringes," *Appl. Opt.* **17**, 2930–2933 (1978).
2. M. Takeda and K. Mutoh, "Fourier transform profilometry for the automatic measurement of 3-D object shapes," *Appl. Opt.* **22**, 3977–3982 (1983).
3. T. L. Pennington, H. Xiao, R. May and A. Wang, "Miniaturized 3D surface profilometer using a fiber optic coupler," submitted to *Optics and Laser Technology*, Jan 2000.
4. Optical Society of America, *Handbook of Optics*, W. G. Driscoll, ed. (McGraw-Hill, New York, 1978).
5. Z. G. Wang, *Wavelength compensation in fused fiber couplers*, Ph.D. Dissertation, (Virginia Polytechnic Institute and State University, Blacksburg, VA, 1996).
6. T. Li, A. Wang, K. Murphy and R. Claus, "White-Light Scanning Fiber Michelson Interferometer for Absolute Position-Distance Measurement," *Opt. Lett.* **20**, 785–787 (1995).

1 Introduction

Surface profilometry has many applications including robotic vision and manufacturing inspection. One popular method of profilometry is fringe projection [1, 2]. The authors are developing a system in which a Young's double pinhole interferometer is used to project fringes onto an object. The fringe positions are then captured on a CCD camera and a combination of phase analysis and triangulation is used to reconstruct the surface [3]. In this system the zero order fringe is used as a calibration point in the reconstruction process. To determine the zero order fringe, two wavelengths are projected through the fiber optic pinhole interferometer – the fringe that does not move is the

zero order fringe, as expressed by Eq. (1).

$$I(x, y) = 2I_o \left[1 + \cos \left(\frac{2a}{d} kx + \Delta\phi \right) \right], \quad (1)$$

where I_o is the initial power out of one fiber (pinhole), $2a$ is the fiber separation, $k = 2\pi/\lambda$, λ is the wavelength, and $\Delta\phi$ is the phase difference of the light at a plane immediately in front of the fibers.

As long as $\Delta\phi$ is constant, the location of the zero order fringe (corresponding to $x = 0$) will be independent of wavelength. However, if the fibers from the coupler to the “pinholes” differ in length, or if the fiber endfaces are not perfectly aligned, then $\Delta\phi$ will be wavelength dependent since

$$\Delta\phi(\lambda_1, \lambda_2) = 2\pi [n_f \Delta L - n_o d] \left(\frac{\lambda_1 - \lambda_2}{\lambda_1 \lambda_2} \right) + \frac{2\pi}{\lambda_2} \Delta n \Delta L, \quad (2)$$

where n_f is the effective refractive index of the fiber core, $\Delta n(\lambda_1, \lambda_2)$ is the change in refractive index due to dispersion, n_o is the refractive index of air, λ_1 and λ_2 are the two wavelengths used to calculate the zero order fringe, and d is the offset between the two fibers endfaces illustrated in Figure 1.

2 Fringe Generator Requirements

The two requirements on the fringe generator (or pinholes) are good fringe visibility and zero order fringe stability at both wavelengths of operation. The wavelengths being used for this system are 633nm (HeNe) and 830nm, primarily because sources and detectors at these wavelengths are readily available at a low cost.

To achieve good fringe visibility, the fiber coupler needs to be approximately a 3dB coupler, which splits the light approximately 50/50 between the two output fibers. To achieve zero order fringe stability at both wavelengths, we need to ensure that the phase difference expressed in Eq. (2) is small. We established a criterion that the phase difference, $\Delta\phi$, must be less than $2\pi/30$, which will ensure that the fringes move less than one pixel when imaged by the CCD camera.

Looking again at Eq. (2), if dispersion is neglected ($\Delta n = 0$), any small length difference could be easily compensated for by adjusting the offset between the fiber endfaces so that $d = n_f \Delta L / n_o$. We note that d must still be less than 0.5mm so that the light diverging from the short fiber endface does not intersect the long fiber. If we include the effects of dispersion and adjust the fiber offset as described, then Eq. (2) is greatly simplified and we can determine the maximum fiber length difference as

$$\Delta L_{\max} = \frac{\lambda_2 \Delta\phi_{\max}}{2\pi \Delta n}. \quad (3)$$

Using Ref. [4, pg. 7–85, Table 16], Δn was determined to be 4.2×10^{-3} . Thus, the maximum fiber length difference we can tolerate is $6.6\mu\text{m}$.

3 Manufacturing Process

A fiber coupler designed to have a 50/50 splitting ratio at both 633nm and 830nm is not a commercial-off-the-shelf item. Hence the first step in manufacturing this fringe generator was to make a coupler with the proper splitting ratio. The process for fabricating a thermally fused biconical tapered coupler is well described in [5]. Briefly, however, two fibers are connected to the two sources. A small section of the fibers are stripped of their jacket and buffer, and twisted together. Using a propane torch, the fibers are

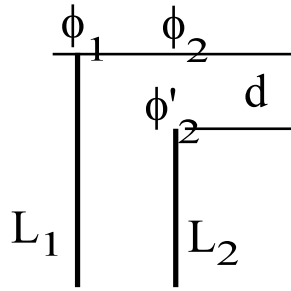


Fig. 1. Schematic of the fiber alignment used to compute the optical path difference using Eq. (2). L_1 is the length of the long fiber, L_2 is the length of the short fiber, d is the normal distance between two lines parallel to the fiber endfaces, ϕ_1 is the phase of the light exiting the long fiber, ϕ_2' is the phase exiting the short fiber and ϕ_2 is the phase of the short fiber's light when it is parallel to the long fiber endface.

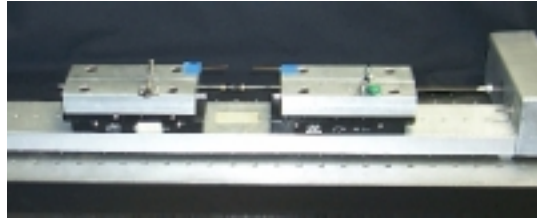


Fig. 2. The coupler manufacturing station used to make the coupler in this system.

then heated and pulled so that they are tapered and fused together. The power out of each fiber is monitored in real time so that the tapering process can be stopped when the splitting ratio is approximately 50/50. Our coupler manufacturing station is shown in Figure 2.

To ensure the fibers are equal lengths, within a few microns, a white light interferometer is used, as shown in Figure 3. This is essentially a fiber optic Michelson interferometer with a broad spectrum superluminescent light emitting diode (SLED) source to inject light into the coupler [6]. The back reflections are then observed by an Ando optical spectrum analyzer. Fringes will develop on this spectrum corresponding to the path difference, which can be measured using:

$$\Delta L = \frac{\lambda_1 \lambda_2}{2n |\lambda_1 - \lambda_2|}, \quad (4)$$

where λ_1 and λ_2 are the wavelengths of any two adjacent peaks of the fringe pattern on the spectrum. In our setup, the two post-coupler fibers are cut so that one is approximately 1mm longer than the other. The two fibers are then mounted onto a polishing machine so that the pressure of each fiber against the lap can be controlled (see Figure 4). The white light interferometer is then used to measure the length difference while the longer fiber is polished.

Two spectra obtained during polishing are shown in Figure 5. Figure 5(a) is the initial spectrum which shows a fringe separation of 0.2nm. This is converted to a fiber length difference using Eq. (4). Doing so yields a length difference of approximately 1mm, which agreed with what we observed by pulling the two fibers taut. A spectrum mid-way through the polishing process is shown in Figure 5(b). The fringe separation has increased to approximately 1nm and the length difference decreased to 230 μ m.

The final spectrum we obtained using this system is shown by the red trace in Figure 6. The fringes readily observed in this trace give a fiber length difference of

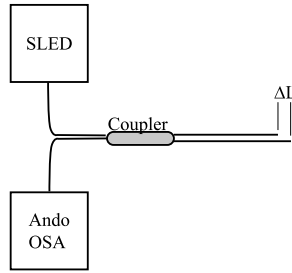


Fig. 3. The fiber length difference is measured using a white light interferometer.

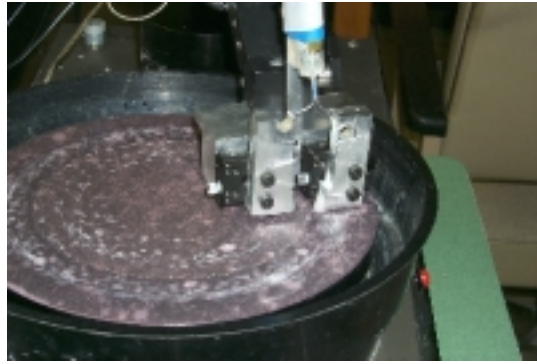


Fig. 4. The fibers are mounted onto the polishing machine so that the pressure of each fiber against the lap can be controlled. Polishing continues until the desired length difference is achieved.

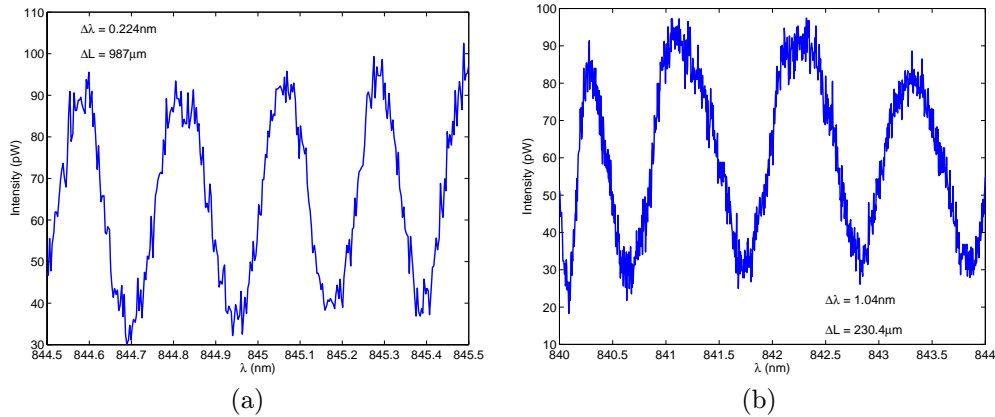


Fig. 5. Sample spectra obtained during the fringe generator manufacturing process. (a) The initial spectrum which shows a fiber length difference of approximately 1mm. (b) A spectrum mid-way through the process; the length difference has decreased to 230 μ m.

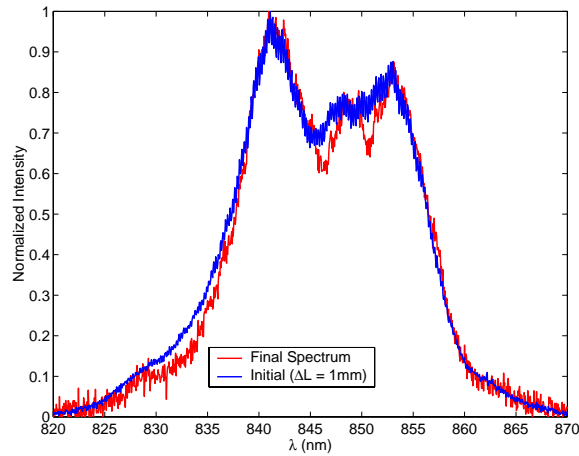


Fig. 6. A comparison of the final spectrum (red) and initial spectrum (blue) taken at the same time as Figure 5(a). The fringes readily observed are noise arising from some other reflection in the system.

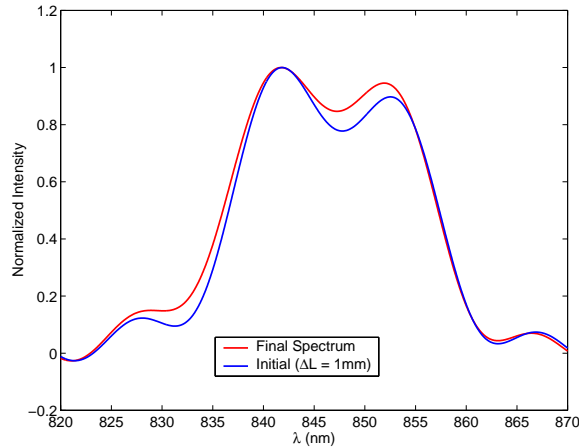


Fig. 7. A low-pass filtered version of a spectra in Figure 6.

approximately $40\mu\text{m}$. However, the blue trace in Figure 6 is a full width spectrum taken at the same time as Figure 5a., when $\Delta L \approx 1\text{mm}$. The actual fringes in this initial (blue) spectrum are of such high frequency they can barely be resolved. If we clean up the envelope of these spectra by running them through a low pass filter, as shown in Figure 7, we observe that they are almost identical. Hence, we conclude that the fringes observed in these spectra result from some other reflection in the system or modal noise in the SLED source. The “true” fringes resulting from the fiber endfaces have a period longer than the SLED spectrum width, which implies that the length difference is less than $6\mu\text{m}$. Further, the amount the fiber was lowered during the polishing process was carefully recorded. These records correlated very well to spectra taken throughout the polishing process and also indicated a length difference less than $6\mu\text{m}$.

Given the limitation of the SLED spectrum width, we could not reliably measure length differences smaller than $6\mu\text{m}$. Hence continuing to polish the fibers would not be useful, especially since the length difference meets the requirement discussed in Section 2. The length difference can now be compensated for by offsetting the fiber endfaces as depicted in Figure 1, without an excessive amount of dispersion induced phase shifting.

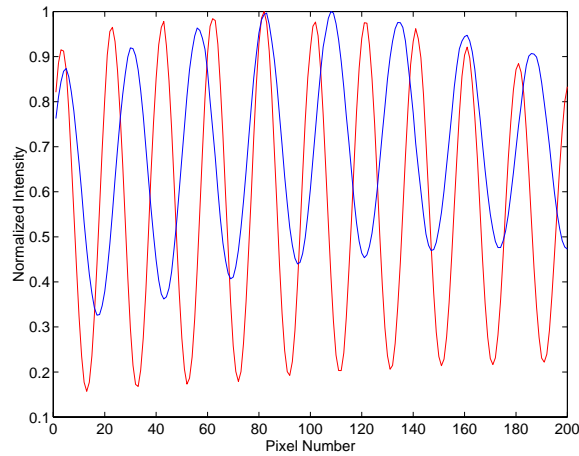


Fig. 8. A cross section of the fringe pattern after the fibers were polished and aligned. The red trace is for the HeNe and the blue trace is for the 830nm laser diode. The zero order fringe is located pixel number 82.

4 Results

After the polishing process was complete, the fibers were removed and each placed on a two-dimensional translation stage, which allowed the fiber separation and endface offset to be controlled. The fibers were aligned and the fringe pattern shown in Figure 8 was observed.

These results indicate that the fibers are properly aligned such that the zero order fringe, aligned with pixel number 82, does not move when the source wavelength is switched between the 633 and 830nm source.

5 Conclusions

In this paper we have described our process for making a Young's double pinhole interferometer. Since we are planning to determine the zero order fringe by using two different wavelengths, stringent requirements were placed on the phase difference of the light exiting the fibers. Using a white light interferometer, we are able to measure the length difference of the fibers during the polishing process. The final length difference measured was approximately $6\mu\text{m}$. The shorter of the two fibers was then pulled back from the other to introduce a phase delay to obtain a final phase difference of less than $2\pi/30$. A plot of the two fringe patterns is provided (Figure 8) which showed the alignment of the zero order fringes.

Acknowledgements

The authors would like to thank Wei Huo for her help in setting up the white light interferometer. Further, the authors appreciate the assistance of Jack Gray and James Wachter in manufacturing the holder used in the polishing process.